

Fatigue properties and fatigue fracture mechanisms of SiC whiskers or SiC particulate-reinforced aluminium composites

CHITOSHI MASUDA, YOSHIHISA TANAKA

National Research Institute for Metals, 2-3-12, Nakameguro, Meguro-ku, Tokyo, Japan

Fatigue properties and fracture mechanisms were examined for three commercially fabricated aluminium matrix composites containing SiC whiskers (SiC_w) and SiC particles (SiC_p) using a rotating bending test. The fatigue strengths were over 60% higher for SiC_w/A2024 composites than that for the unreinforced rolled material, while for the SiC_p/A357 composites, fatigue strengths were also higher than that for the unreinforced reference material. For the SiC_p/A356 composites at a volume fraction of 20%, the fatigue strength was slightly higher than that of the unreinforced material. Fractography revealed that the Mode I fatigue crack was initiated by the Stage I mechanism for the SiC_w/A2024 and SiC_p/A357 composites, while for the SiC_p/A356 composite, the fatigue crack initiated at the voids situated beneath the specimen surfaces. On the other hand, the fatigue crack propagated to the whisker/matrix interface following the formation of dimple patterns or the formation of striation patterns for SiC_w/A2024 composites, while for the SiC_p/A356 and SiC_p/A357 composites the fatigue crack propagated in the matrix near the crack origin and striation patterns were found. Near final failure, dimple patterns, initiated at silicon carbide particles, were frequently observed. Mode I fatigue crack initiation and propagation models were proposed for discontinuous fibre-reinforced aluminium composites. It is suggested that the silicon carbide whiskers or particles would have a very significant effect on the fatigue crack initiation and crack propagation near the fatigue limit.

1. Introduction

A major part of the effort in aluminium matrix composites has been directed towards the development of high-performance composites, with very high strength and high moduli [1]. It has been reported that the tensile strengths of SiC whisker-reinforced aluminium composites were superior to those of the matrix alloys [1-7], while the tensile ductility [1, 3, 4, 6] and fracture toughness [1, 4] of those composites were much lower than those of the matrix alloys. For SiC particulate-reinforced aluminium composites, the tensile strengths were equivalent or superior to those for SiC whisker-reinforced aluminium composites [6, 7].

On the other hand, the fatigue strengths at 10^7 cycles were about 50%–70% higher for 6061 and 7075 aluminium composites reinforced by 20% or 15% SiC whiskers, than those for the matrix alloys [7]. The fatigue crack propagation rates were about one order of magnitude lower for 6061 aluminium composites reinforced with 20% SiC whiskers than those for matrix alloys in a direction transverse to the aligned whiskers [7]. It has also been reported that for SiC whisker-reinforced 6061 aluminium composites, the fatigue crack propagation rates were inferior to those for the matrix alloys [8]. The fatigue thresholds of SiC whisker-reinforced aluminium composites were about the same as the matrix alloys [9]. Those results are

inconsistent. It is concluded that the fatigue crack propagation mechanism is not yet clear, and the fatigue life cannot be predicted on the basis of the data reported for SiC whisker-reinforced aluminium composites.

For the SiC particulate-reinforced aluminium composites, the fatigue strength was equivalent to or lower than that for a matrix alloy in the long range of life over about $N_f = 5 \times 10^6$ cycles [7]. Fatigue crack propagation rates for SiC particulate-reinforced aluminium composites containing fine SiC particles were higher than those for the matrix alloys in a given stress intensity factor range, ΔK , while the fatigue crack propagation properties for those composites containing coarse SiC particles were very similar for the matrix alloys [10].

It is considered that short-fibre-reinforced composites containing SiC whiskers or particles are rather isotropic materials and more easy to forge or extrude in comparison to the long-fibre-reinforced composites. Moreover, the ratio of tensile strength to density for those composites was higher than that for titanium alloys [1].

In this study, the fatigue strength was evaluated and the Mode I fatigue crack initiation and propagation mechanisms are discussed for SiC whisker or SiC particulate-reinforced aluminium composites.

TABLE I Chemical compositions (wt %)

Material	Si	Fe	Cu	Mn	Mg	Cr	Zn	Ti
SiC _w /A2024 (10%)	8.23	0.23	3.62	0.65	1.39	0.005	0.030	–
SiC _w /A2024 (20%)	14.66	0.24	3.31	0.47	1.17	0.022	0.017	–
SiC _p /A356 (10%)	13.12	0.078	0.007	0.007	0.61	–	0.004	–
SiC _p /A356 (20%)	20.30	0.079	0.007	0.007	0.53	–	0.003	–
SiC _p /A357 (15%)	16.60	0.085	0.016	0.003	0.88	–	0.003	–
SiC _p /A357 (20%)	20.79	0.088	0.011	0.002	0.72	–	0.002	–
A2024	0.50	0.50	3.8 ~ 4.9	0.3 ~ 0.9	1.20 ~ 1.80	0.1	0.25	–
A356 ⁽¹⁾	6.5 ~ 7.5	0.11	0.10	0.05	0.30 ~ 0.40	–	0.05	0.20
A357 ⁽¹⁾	6.5 ~ 7.5	0.12	0.10	0.05	0.45 ~ 0.70	–	0.05	0.10 ~ 0.20
AC4CH	7.40	0.10	–	–	0.33	–	–	0.10

2. Experimental procedure

2.1. Materials

Three types of material were used in this study. The first was an SiC whisker (SiC_w)-reinforced composite (SiC_w/A2024), the second and third were SiC particulate (SiC_p)-reinforced composites (SiC_p/A356 and SiC_p/A357). The volume fractions (V_f) of SiC whisker or SiC particles were 10%, 15% and 20%. The SiC_w/A2024 composite was fabricated by powder metallurgy and the SiC_p/A356 and SiC_p/A357 composites were made by the casting method. The whiskers were β -SiC with diameter ranging 0.1–1.0 μm and original lengths up to about 15 μm .

The whiskers were blended with 300 mesh commercially available inert gas-atomized powders of 2024 aluminium alloys. The composites were formed by cold compaction followed by hot pressing at temperatures above the solidus of the matrix alloys under degassed conditions, to form as-pressed billet materials. The billets were extruded to form the bar. The extrusion ratio was about 10. SiC_p/A356 and SiC_p/A357 composites were fabricated by the Dural Aluminium Composite Corporation.

Table I gives the chemical compositions of the three composites. The three composites were heat treated in the T6 condition. Fig. 1 shows the microstructures of

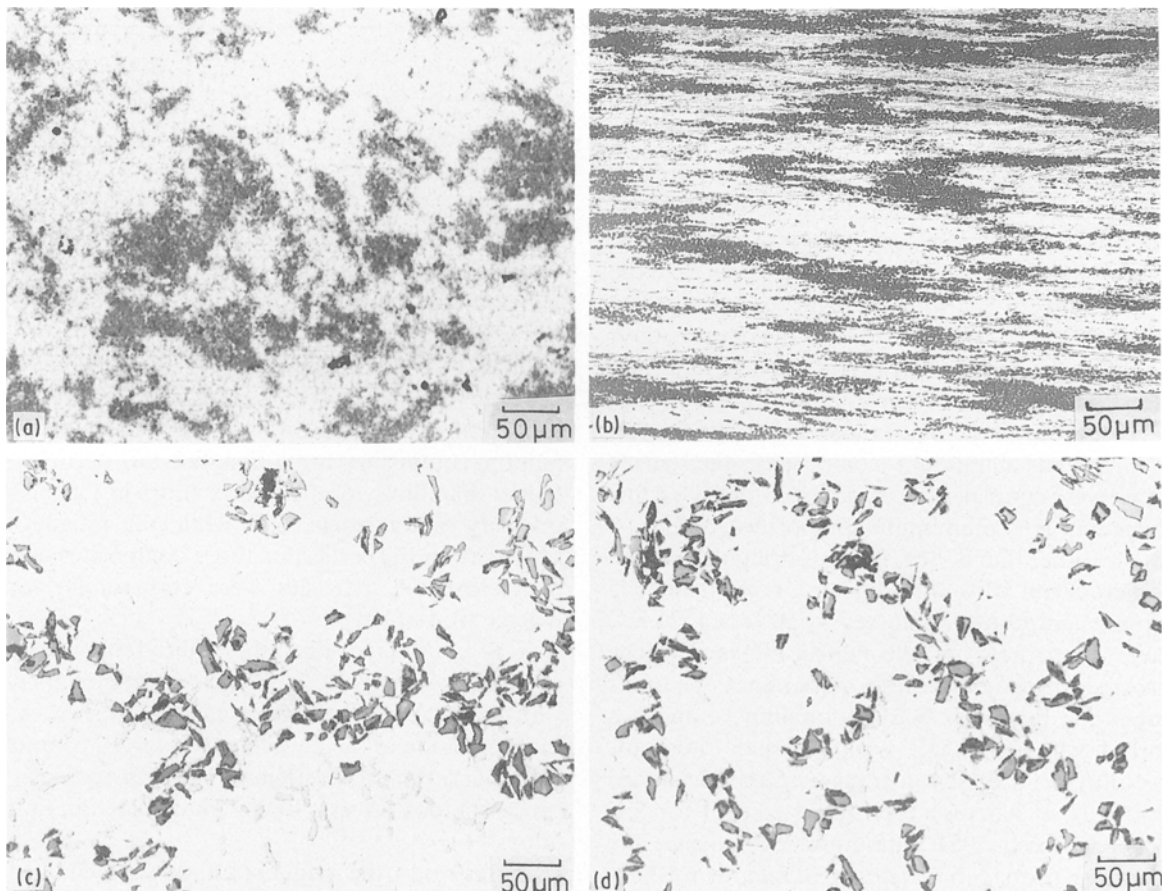


Figure 1 Micrographs of discontinuous fibre-reinforced composites. (a) SiC_w(10)/A2024 in cross-section. (b) SiC_w(10)/A2024 in section parallel to the longitudinal direction. (c) SiC_p(10)/A356 in cross-section. (d) SiC_p(15)/A357 in cross-section.

TABLE II Tensile properties

Material	Thermal treatment	0.2% yield stress (MPa)	Tensile strength (MPa)	Elongation (%)	Modulus (GPa)
SiC _w /A2024 (10%)	Fab.	221	407	2.6	89
	T6	408	630	4.3	92
	T6	515	720	1.6	121
SiC _p /A356 (10%)	Fab.	149	193	9.2	80
	T6	353	387	2.2	76
SiC _p /A356 (20%)	Fab.	125	190	4.5	92
	T6	370	394	0.8	96
SiC _p /A357 (15%)	Fab.	103	165	7.6	83
	T6	345	372	1.6	79
SiC _p /A357 (20%)	Fab.	124	196	5.1	100
	T6	378	402	0.95	98
A2024	T6	390	480	10.4	75
A356 ⁽¹¹⁾	T6	206	284	10.0	–
A357 ⁽¹¹⁾	T6	275	343	10.0	–
AC4CH	T6	215	275	6.9	–

three composites. In Fig. 1a dark areas show the whisker-rich zones, while white areas are the whisker-poor zones for SiC_w/A2024 composites ($V_f = 10\%$). In the cross-section normal to the specimen axis, SiC whisker-rich zones elongated to the extruded direction were found, such as the long fibres shown in Fig. 1b. Fig. 2 shows the microstructure of the SiC whiskers contained in the 10%-SiC_w/A2024 composite, where the acicular-like white bars are the SiC whiskers aligned parallel to the extrusion direction. The average size of SiC whiskers is about 0.57 μm diameter or about 4.7 μm long.

For SiC_p/A356 (10%) and SiC_p/A357 composites ($V_f = 15\%$) dark particles are seen, which are the SiC particles shown in Fig. 1c and d. Triangular or rectangular SiC particles are found in these micrographs. The average sizes of SiC particles for 10%-SiC_p/A356 composites was about 5–10 μm long, while for 20%-SiC_p/A356 and 15%- or 20%-SiC_p/A357 composites, the sizes were about 20–30 μm long.

2.2. Mechanical tests

The tensile and fatigue test specimens were cut from the bars or ingots and roughly machined before heat

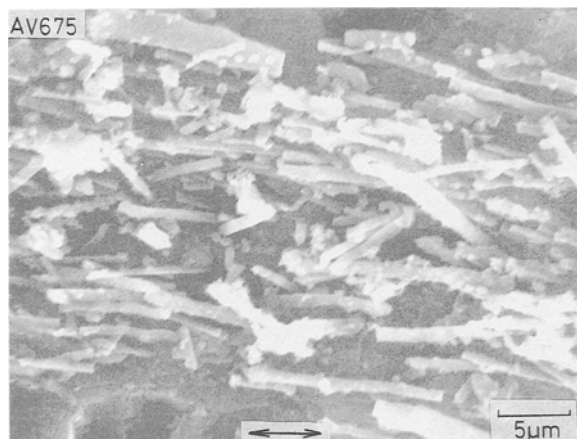


Figure 2 Micrograph of SiC whiskers contained in SiC_w(10)/A2024 composites.

treatment. After heat treatment, the fatigue specimens were machined again and those surfaces were polished by diamond paste. Tensile tests were conducted on round tensile specimens 140 mm long with 50 mm long reduced section, 10 mm diameter.

The tensile crosshead speed was 0.5 mm min⁻¹ to the 0.2% yield stress and then 2 mm min⁻¹ until failure. The elastic modulus was determined using a strain gauge bonded to a specimen surface. The fatigue tests were performed on round specimens 130 mm long with 20 mm long reduction section, 6 mm diameter, under rotating bending conditions (50 Hz) in laboratory air. The fatigue fracture surface was examined using a scanning electron microscope (SEM).

3. Results and discussion

3.1. Mechanical properties

Tensile properties of three composites under the T-6 heat-treatment condition, as-fabricated or as-cast, are given in Table II. The tensile strength and Young's modulus of three composites heat treated in the T6 condition were higher than those of the matrix alloys [11], while those ductilities decreased in comparison to the matrix alloys.

Fig. 3 shows the variation of the tensile strengths of composites with the volume fractions of SiC whiskers or SiC particles. The two straight lines show the estimated values using the following equations:

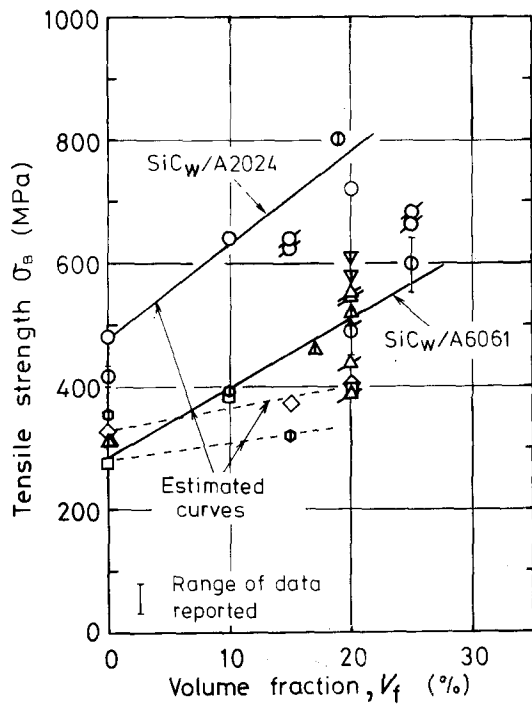
$$\sigma_c = \sigma_w V_f F(l_c/l) C_o + \sigma_m (1 - V_f) \quad (1a)$$

$$F(l_c/l) = 1 - l_c/2l \quad (l_c < l) \quad (1b)$$

$$= l/2l_c \quad (l_c > l)$$

$$l_c/d = \sigma_w/\sigma_m \quad (1c)$$

where σ_c , σ_w and σ_m are the tensile strength of composites, whiskers and matrix alloys, V_f is the volume fractions, $F(l_c/l)$ is the factor of fibre length and C_o is the orientation factor of whiskers. l_c and l are the critical length and average length of fibres. The values of strength of whiskers or matrix alloys are 13.7 GPa (shown in the catalogue) and 480 MPa as shown in



Symbol	Material
○	SiC _w /A2024
⊙ [1]	SiC _w /A2024
⊙ [2]	SiC _w /A2024
□	SiC _p /A356
◇	SiC _p /A357
△ [4]	SiC _w /A6061
△ [2]	SiC _w /A6061
▽ [5]	SiC _w /Al-Li
⊕ [12]	SiC _p /Al-Cu-Mg

Figure 3 Relationship between tensile strength and volume fraction in aluminium matrix composites.

Table II. The diameter, d , and length l of whiskers used were the values given in Section 2.1. The value of l_c is calculated from Equation 1a-c ($= 14 \mu\text{m}$). The values of strength of SiC whisker-reinforced composites at the volume fraction used, are about 630 and 770 MPa. These results are in good agreement with the experimental data.

On the other hand, for SiC particulate-reinforced composites, the tensile strengths were also estimated from Equation 1a-c. In Fig. 3 the dashed lines show the estimated values. The tensile strength of SiC particles was not reported. A value of 12 GPa was used, with an average length and diameter of 30 and 10 μm , respectively. The estimated lines are lower than the experimental data. It is suggested that the increases in the tensile strength for SiC particle-reinforced composites could be described by the same equation for the SiC whisker-reinforced composites.

The effect of the volume fraction of SiC whiskers or SiC particles on the elastic modulus was slightly significant in the range of the volume fraction from 10%–20%, while the ductility for composites was less than that for the matrix alloys. The elastic modulus increased with the increasing volume fraction.

3.2. Fatigue properties

The stress-number of cycles to failure diagram showing the rotating bending fatigue properties of composites is shown in Fig. 4, where the lines are

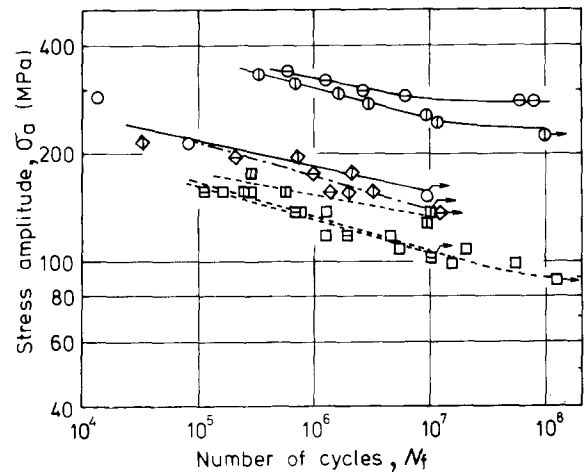


Figure 4 S-N curves for discontinuous fibre-reinforced composites. Material (V_f , %): (○) A2024; (⊙) SiC_w/A2024 (10); (⊕) SiC_w/A2024 (20); (□) JIS AC4CH; (▣) SiC_p/A356 (10); (⊞) SiC_p/A356 (20); (⊕) SiC_p/A357 (15); (⊕) SiC_p/A357 (20).

estimated by the regression method on log-log coordinates paper. For SiC_w/A2024 composite and AC4CH aluminium alloy, the fatigue limit was clearly found up to about 10^8 cycles, while for SiC_p/A356 and SiC_p/A357 composites the fatigue limit was not seen up to about 10^7 cycles. The fatigue strengths at 10^5 , 10^6 and 10^7 cycles estimated are listed in Table III. The fatigue strength of SiC_w/A2024 composites was much higher than that of the A2024 matrix alloy fabricated by rolling. For SiC_p/A356 composites, the fatigue strength at $V_f = 10\%$ was higher than that for AC4CH matrix alloy, while at $V_f = 20\%$ the fatigue strength was equivalent to that of the matrix alloy. For SiC_p/A357 composites the fatigue strength is equivalent for the two volume fractions of SiC particles of 15% and 20%.

Fig. 5 shows the variation between the ratio of fatigue strength of composites, σ_{wc} , to the aluminium matrix alloys, σ_{wo} , σ_{wc}/σ_{wo} , at the number of cycles to failure of 10^7 , and the volume fraction of SiC whiskers or SiC particles. For the SiC_w/A2024 composite, the fatigue strength increases with increasing volume fraction of SiC whiskers, but the increase of the fatigue strength of the composites tends to saturate over a volume fraction of 20%.

For SiC_p/A357 composites, the fatigue strength also increases with volume fraction of SiC particles, and tends to become constant over a volume fraction of

TABLE III Fatigue strength (MPa)

Material	10^5	10^6	10^7
SiC _w /A2024 (10%)	380	303	251
SiC _w /A2024 (20%)	—	322	283
SiC _p /A356 (10%)	178	152	132
SiC _p /A356 (20%)	161	127	105
SiC _p /A357 (15%)	202	174	152
SiC _p /A357 (20%)	213	168	152
A2024	207	164	153
A356 ¹¹⁾	—	—	88
A357 ¹¹⁾	—	—	107
AC4CH	128	105	101

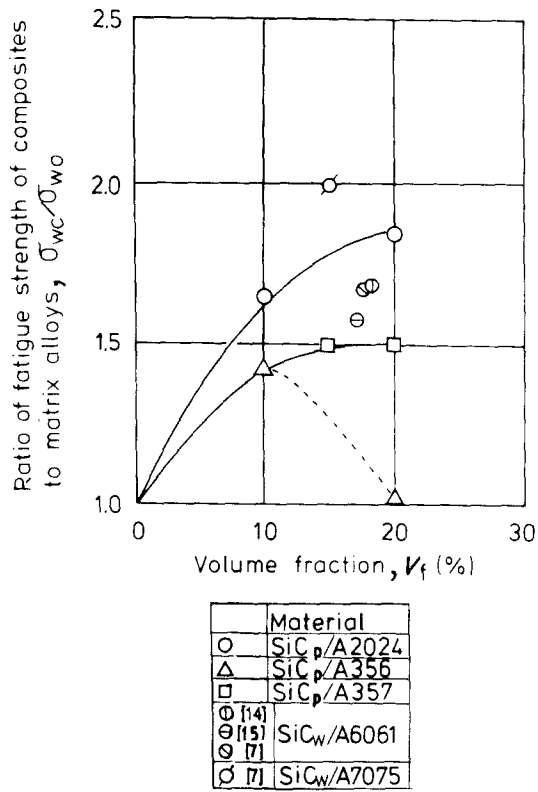


Figure 5 Variation of ratio of fatigue strength of composites to matrix alloys to the volume fraction.

15%, while for SiC_p/A356 composites the fatigue strength tends to a maximum at a volume fraction of 10%. For this composite at a volume fraction of 20%, the fatigue strength was slightly higher than that of the matrix alloys. The reason for this is that the fatigue crack initiated at the voids beneath the specimen surfaces, as mentioned below.

Fig. 6 shows the variation of the ratio of fatigue strength at the number of cycles to failure of 10⁷, σ_{wc} or σ_{w0} , to the tensile strength, σ_B , and the volume fraction. The data obtained in this study were contained in the range of σ_w/σ_B from 0.34–0.40, while the reference data for the composites were about 0.38. For high-strength aluminium alloys [16] the average value of σ_w/σ_B was 0.38 and for cast aluminium alloys [16] that value was about 0.35.

It is considered that the difference in the average values of σ_w/σ_B between high-strength aluminium alloys and cast aluminium alloys would be caused by the fatigue crack origins, that is, for the former materials the crack would initiate by Stage I mechanisms, while for the latter materials the crack would begin at shrinkage holes on the specimen surfaces. For the SiC_p/A356 composites the value of σ_w/σ_B was lower than the other two composites, due to fatigue crack initiation at voids at or beneath the specimen surfaces.

Hasson *et al.* [17] have reported the fatigue properties for the 20%-SiC_w/A6061 and 25%-SiC_p/A6061 composites. The ratio of fatigue strength at 10⁷ cycles to tensile strength calculated for these composites is about 0.23. This value was much smaller than those for SiC_w/A2024 or SiC_p/A357 composites obtained in this study. On the other hand, Harris [18] has also reported the fatigue properties for a discontinuous

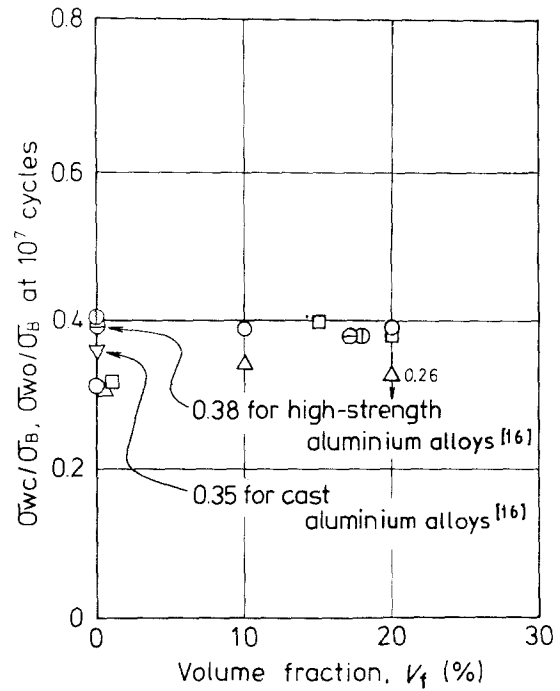


Figure 6 Relationship between fatigue strength to tensile strength and the volume fraction for T6 conditions. (○) SiC_w/A2024; (△) SiC_p/A356; (□) SiC_p/A357; (▽) AC4CH; (◇) SiC_w/A6061 [14]; (⊕) SiC_w/A6061 [15].

alumina short-fibre-reinforced aluminium composite (20%-Al₂O₃/A2619). The ratio of fatigue strength to tensile strength calculated was about 0.39. This value was equivalent to our data.

It is concluded that the role of SiC whiskers or SiC particles contained in the composites could be increasing resistance to fatigue crack initiation, but if there are voids situated beneath the specimen surfaces, the fatigue crack would initiate at those voids and the fatigue strength would not increase in comparison to that of the matrix alloys.

3.3. Fractography

Fig. 7 shows the macrofractographs of three composites and AC4CH aluminium alloys fabricated by casting methods, compared to the A356 aluminium alloys. In the fractographs the fatigue crack origins are indicated by arrows. For SiC_w/A2024 and SiC_p/A357 composites, only one fatigue crack initiation site was found, while for SiC_p/A356 composite many fatigue crack origins were seen. For AC4CH aluminium alloy a large shrinkage hole was found at the specimen surface. In this case the size of the crack origins was about 0.2–1.0 mm.

Fig. 8 shows microfractographs of the fatigue crack origins for the three composites. For the SiC_w/A2024 and SiC_p/A357 composites, voids or shrinkage holes were not observed at the fatigue crack origins. For these composites, Stage I-type cracking was found as shown in Fig. 8a and c indicated by B and A. For the SiC_w/A2024 composite, a rub mark, A, was also seen at the crack origin near the specimen surface, except for the Stage I-type crack, as indicated by B in Fig. 8a.

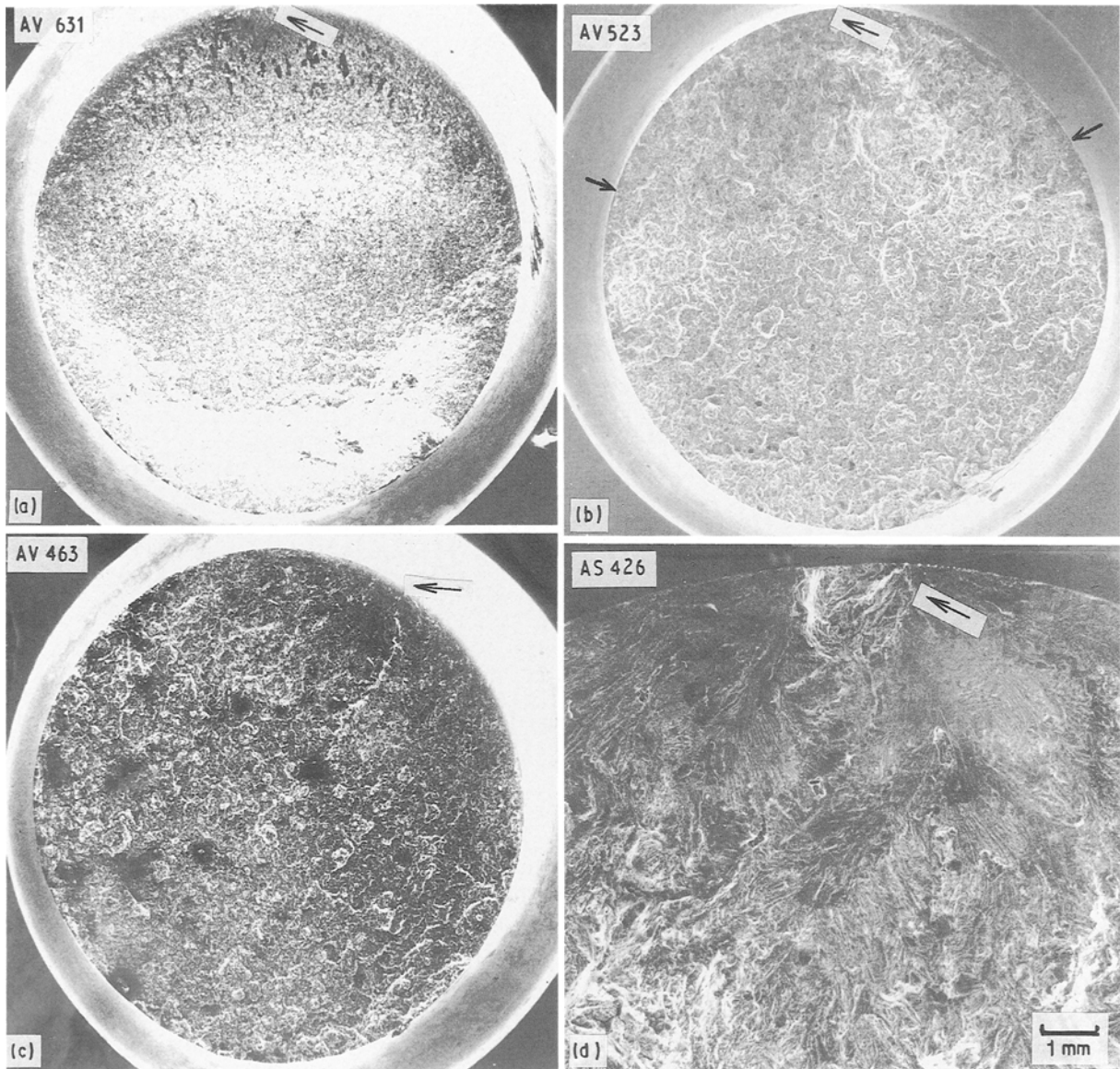


Figure 7 Macrofractographs of fatigue fracture surfaces. (a) $\text{SiC}_w(10)/\text{A2024}$ ($\sigma_a = 245 \text{ MPa}$, $N_f = 1.17 \times 10^7$). (b) $\text{SiC}_p(10)/\text{A356}$ ($\sigma_a = 137 \text{ MPa}$, $N_f = 1.01 \times 10^7$). (c) $\text{SiC}_p(15)/\text{A357}$ ($\sigma_a = 157 \text{ MPa}$, $N_f = 2.03 \times 10^6$). (d) AC4CH ($\sigma_a = 98 \text{ MPa}$, $N_f = 2.49 \times 10^6$).

For $\text{SiC}_p/\text{A356}$ composite, a void situated beneath the specimen surface was observed, as indicated by the arrow. In particular, many silicon carbide particles were seen in that void. It is suggested that the region containing many silicon carbide particles could not be filled with A356 aluminium matrix alloy, because of the lack of wetting.

Fig. 9 shows the microfractograph of Stage I crack observed at a tilt angle of 30° at the same site as shown in Fig. 8a for the $\text{SiC}_w/\text{A2024}$ composite. In Fig. 8a, a rub-mark, A, was also found, while Stage I crack, B in Fig. 8a, was hardly seen. It is concluded that the Stage I crack was inclined to the specimen axis. In Fig. 9 taken at high magnification of the Stage I crack for the $\text{SiC}_w/\text{A2024}$ composites, areas where small precipitation-like patterns gathered, were found. These areas show whisker-rich zones and the small precipitation-like patterns could be assembled at the edge of the whiskers. On the other hand, small precipitation-free zones were also seen. These zones could be

whisker-free ones. It is suggested that the fatigue crack would propagate to the whisker/matrix interfaces.

A fatigue crack initiation mechanism has not been proposed for SiC whisker- or SiC particulate-reinforced aluminium composites. For aluminium alloys, Forsyth [19] has proposed a fatigue crack initiation mechanism based on the extrusion mechanism. For SiC whisker- or SiC particulate-reinforced aluminium composites, fractography reveals the same fatigue crack initiation mechanism as that proposed by Forsyth. In case of $\text{SiC}_p/\text{A356}$ composite with small voids situated beneath the specimen surfaces, the fatigue crack initiates from those voids.

Fig. 10 shows the microfractographs of fatigue crack propagation regions for $\text{SiC}_w/\text{A2024}$ composite. For the $\text{SiC}_w/\text{A2024}$ composites, dimple patterns were frequently found on the whole fatigue surface from near the crack origin to final failure. The striation patterns were occasionally observed among the dimple patterns as shown in Fig. 10b. For the same

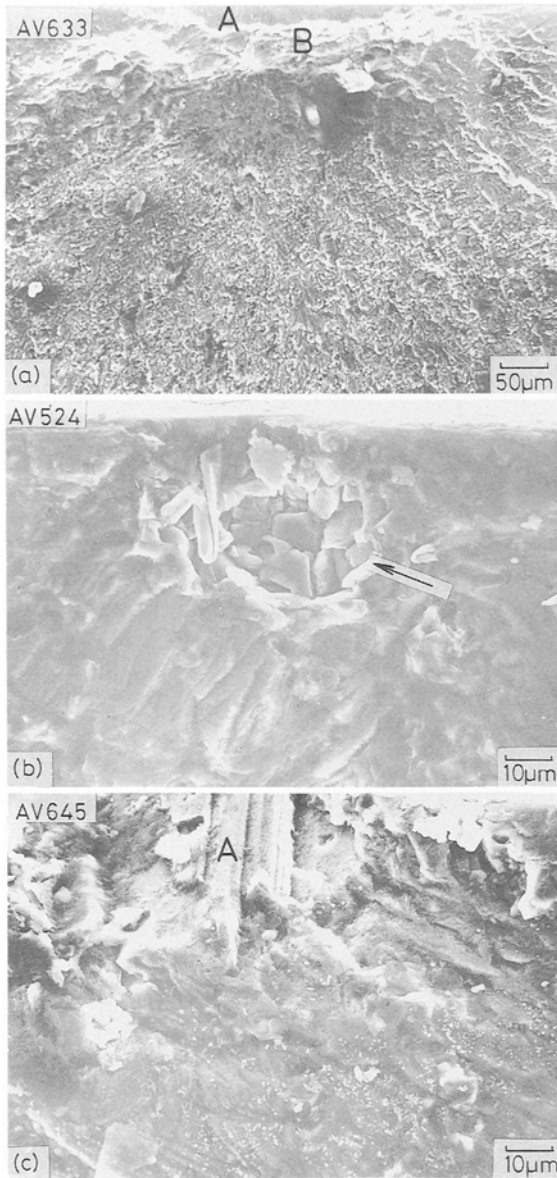


Figure 8 Microfractographs of fatigue crack origin. (a) $\text{SiC}_w(10)/\text{A2024}$ ($\sigma_a = 245 \text{ MPa}$, $N_f = 1.17 \times 10^7$). (b) $\text{SiC}_p(10)/\text{A356}$ ($\sigma_a = 137 \text{ MPa}$, $N_f = 1.01 \times 10^7$). (c) $\text{SiC}_p(15)/\text{A357}$ ($\sigma_a = 157 \text{ MPa}$, $N_f = 2.03 \times 10^6$).

composite at a volume fraction of 20%, dimple patterns were frequently observed on the fatigue fracture surfaces from near the fatigue crack origin to the final failure. It has been reported that fatigue fracture surfaces were covered by dimple patterns and SiC whisker debris for SiC whisker-reinforced A6061-T6 composites at the volume fraction of 20%.

For $\text{SiC}_p/\text{A356}$ composites, the fatigue fracture surfaces were very flat and striation patterns were observed. For these composites the dimple patterns were rarely seen near the fatigue crack origin except for near the final failure. The dimple patterns were initiated at silicon carbide particles. Shang *et al.* [10] have reported that SiC particles were found at a lower stress intensity factor on the surfaces for SiC particle-reinforced aluminium composites ($\text{SiC}_p/\text{MB78}$). They also pointed out that cracked SiC particles were also seen. The SiC particles were rarely observed for $\text{SiC}_p/\text{A356}$ and $\text{SiC}_p/\text{A357}$ composites in this study.

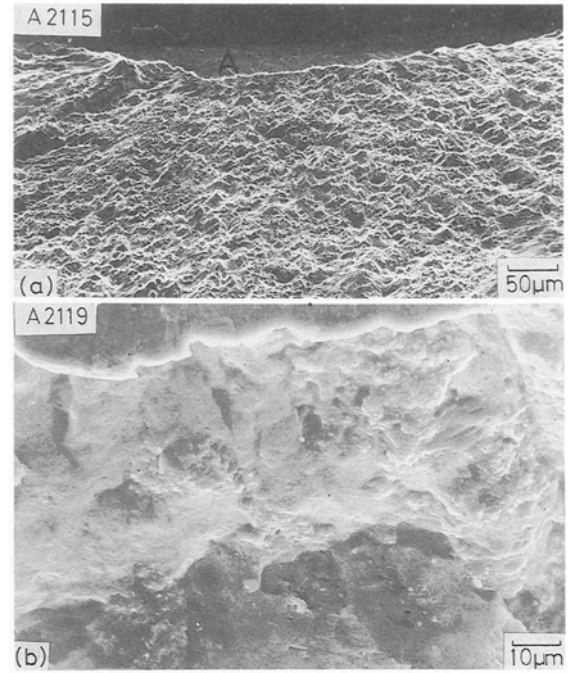


Figure 9 Microfractograph of fatigue crack origin for the $\text{SiC}_w(10)/\text{A2024}$ composite ($\sigma_a = 254 \text{ MPa}$, $N_f = 9.26 \times 10^6$).

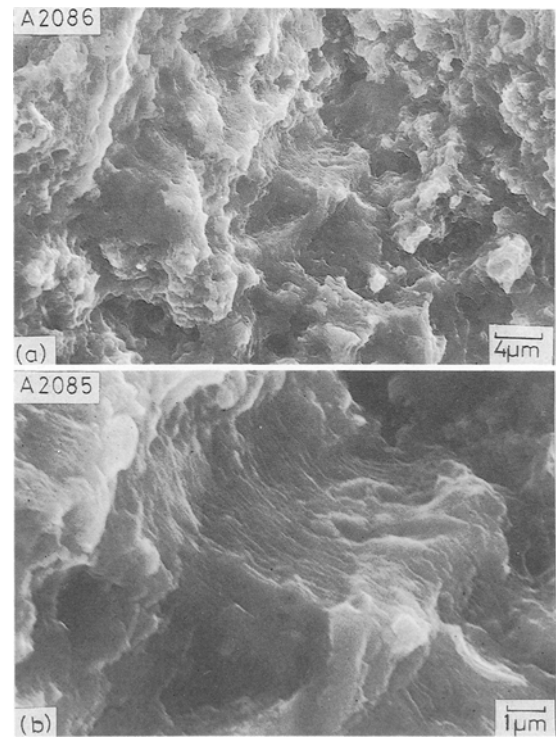


Figure 10 Microfractographs of fatigue crack propagation region for $\text{SiC}_w(10)/\text{A2024}$ composite ($\sigma = 254 \text{ MPa}$, $N_f = 9.26 \times 10^6$).

Because of the very small crack propagation region the stress intensity factor suddenly increased with increasing crack length.

Fig. 11 shows the fish-eye failure observed on the fatigue fracture surface for $\text{SiC}_p(20)/\text{A356}$ composite. These patterns were frequently found near the specimen surfaces. As mentioned in Section 3.2, it is suggested that the fatigue strength was very low for the

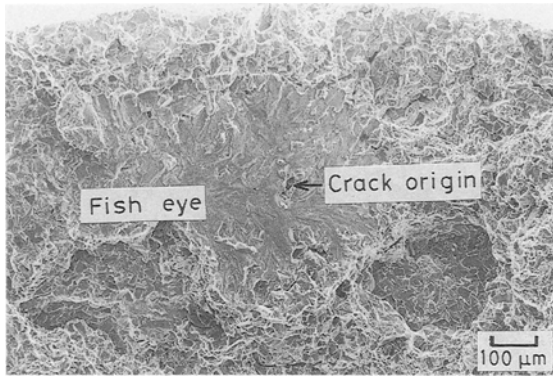


Figure 11 Fish-eye failure for the $\text{SiC}_p(20)/\text{A356}$ composite ($\sigma_a = 117 \text{ MPa}$, $N_f = 1.95 \times 10^6$).

$\text{SiC}_p(20)/\text{A356}$ composite compared to the same composite containing SiC particles of 10%, because of the fish-eye failure.

3.4. Mode I fatigue crack initiation and propagation mechanisms for short-fibre-reinforced composite

Fig. 12 shows the Mode I fatigue crack initiation mechanism for $\text{SiC}_w/\text{A2024}$ composites. The fatigue crack is formed by a slip deformation mechanism for the specimen surface (Stage I crack). When the whiskers are very long in comparison to the plastic zone size, the crack initiated from the specimen surface propagates to the whisker-rich zones and the crack is arrested by aligned whiskers. The crack has to cut through the whiskers or the crack propagates between the whisker/matrix interface. As the Stage I crack is

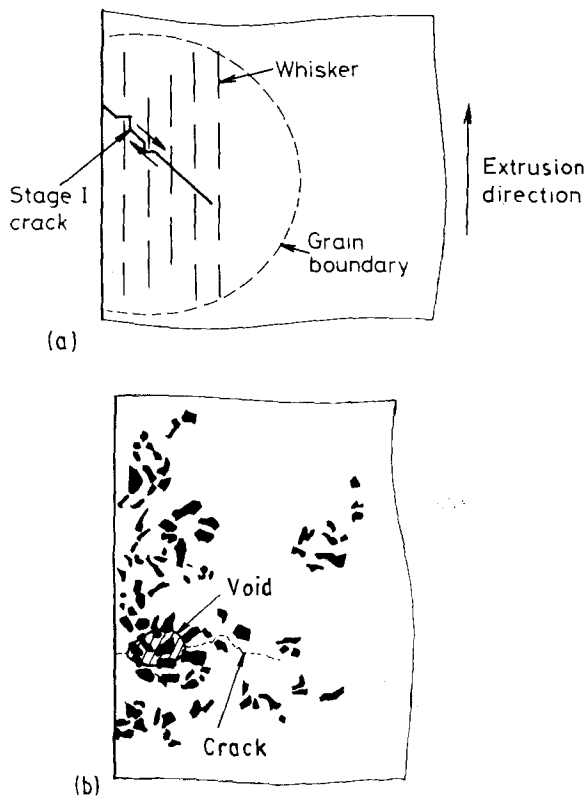


Figure 12 Fatigue crack initiation model for composites.

formed by Mode II or III, the Stage I crack rarely opens. It is considered that the role of whiskers would be to resist the Mode I fatigue crack initiation.

For the $\text{SiC}_p/\text{A356}$ composite, the fatigue crack would initiate at the voids situated at or beneath the specimen surfaces as shown in Fig. 12b. If the voids are not at nor beneath the specimen surfaces, the fatigue crack would initiate by Stage I mechanism [19]. For $\text{SiC}_p/\text{A357}$ composite at the crack origin, a Stage I crack was observed as mentioned above. It is suggested that the voids contained in $\text{SiC}_p/\text{A357}$ composite would be fewer than those of $\text{SiC}_p/\text{A356}$ or the size of $\text{SiC}_p/\text{A357}$ composite would be smaller than that of $\text{SiC}_p/\text{A356}$ composite.

Fig. 13 shows the fatigue crack propagation mechanism. In the case of a small crack or lower stress level, the size of SiC whisker length is larger than the cyclic plastic zone size formed at the crack tip. The fatigue crack reaches the whisker-rich zone and may be arrested by the whiskers as shown in Fig. 6a. At the edge of the whiskers, stress-concentrated dimple patterns would be formed. After the dimple pattern formed at the whiskers contained in the whisker-rich zone, the crack would start to propagate by a striation mechanism in the whisker-poor zone. Under these conditions, fatigue crack propagation rates would be lower than those of unreinforced materials.

In the case of a larger crack length or higher stress level, many whiskers are contained in the cyclic plastic zone and many dimple patterns would be formed around the whiskers ahead of the main crack, as shown in Fig. 13b. The main crack would link to the dimple patterns formed ahead of the main crack. Therefore, fatigue crack propagation rates would be higher than that of unreinforced materials. At a volume fraction of 20%, the whisker-poor zone would be narrow in comparison to that at the volume fraction of 10%. Then the fatigue crack would be propagated

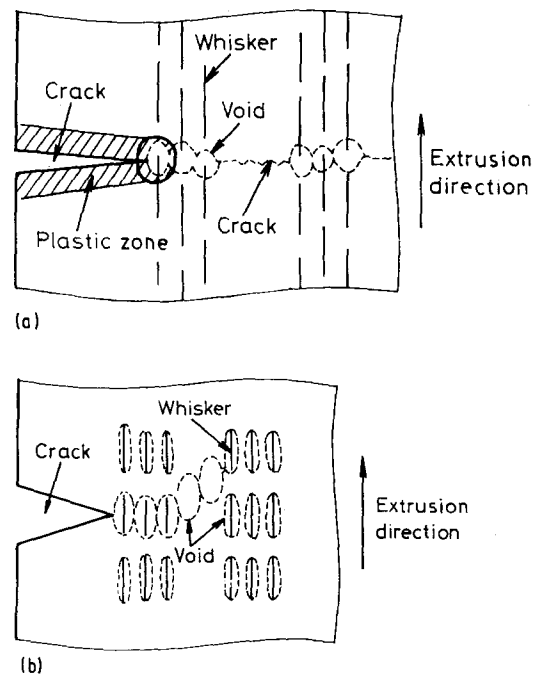


Figure 13 Fatigue crack propagation model in the lower stress level.

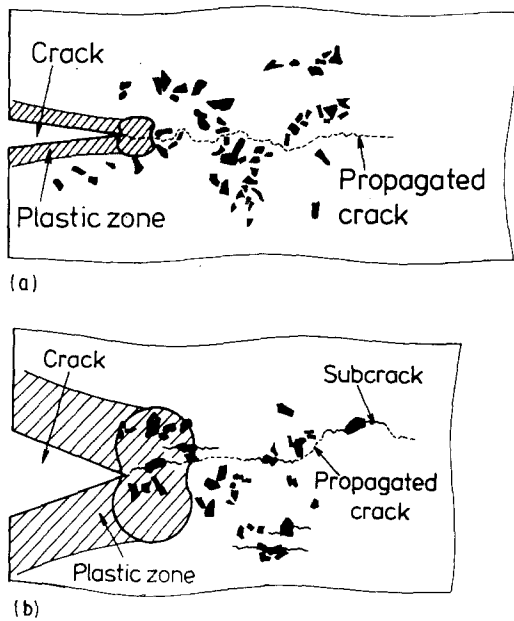


Figure 14 Fatigue crack propagation model in the higher stress level.

at the matrix/whisker interfaces. Therefore, the fracture toughness would be lower at a volume fraction of 20% than that at $V_f = 10\%$. It is suggested that the fatigue crack propagation rates for a given stress condition would be higher at $V_f = 20\%$ than that at $V_f = 10\%$.

On the other hand, for SiC particle-reinforced composites, the fatigue crack would keep away from the particles in the case of the smaller crack length or lower stress levels shown in Fig. 14a. In the case of a large crack length, the subcrack initiated at the particles in front of the main crack and the crack would link to the subcrack, as shown in Fig. 14b.

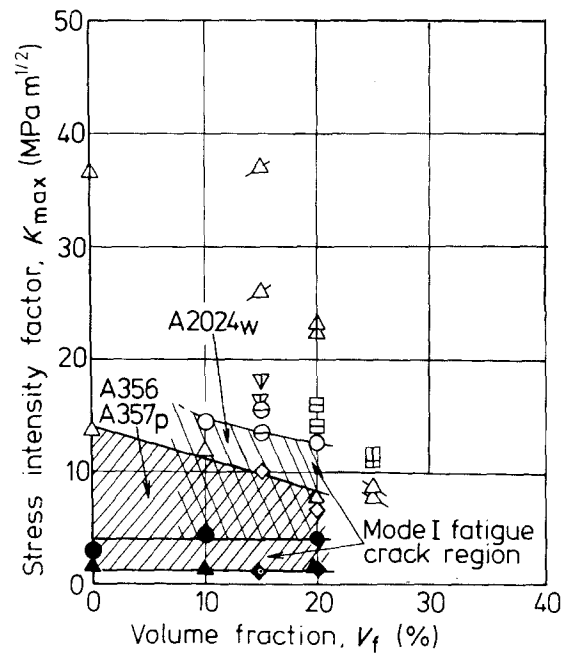
Shang *et al.* [10] have proposed a fatigue crack propagation mechanism for SiC particulate-reinforced aluminium composites (20%-SiC_p/MB78). They considered that the high levels of crack closure were induced by the roughness of the fracture surfaces in part from decohesion around large particles near the fatigue threshold, and fatigue crack propagation rates were decelerated, while at high stress intensity levels the cracking of particles ahead of the crack tip could both accelerate and decelerate crack growth.

3.5. Mode I fracture mechanics of fatigue crack initiation or final failure

Fig. 15 shows the maximum stress intensity factor at the onset of Mode I fatigue crack start or final crack start. In the same figure, the values of fracture toughness are also plotted for the SiC whisker-reinforced composites reported. The maximum stress intensity factor of the onset of Mode I cracking was calculated from Equation 2.

$$K_{max} = (2.24/\pi)\sigma_{max}(\pi a)^{1/2} \quad (2)$$

The fatigue crack length at onset of the Mode I crack start, a_i , and final fatigue crack depth, a_f , were measured on the fractographs from the Stage I crack depth,



K_{th}	K_{Ic}	K_{Tc}	Materials
●	○	⊖ [1]	SiC _w /A2024
		△ [4]	SiC _w /A6061
		△ [7]	
		△ [7]	
		▽ [7]	SiC _w /A5456
		⊖ [10]	SiC _p /MB78
		⊖ [7]	SiC _p /A6061
▲	△		SiC _p /A356
	◇		SiC _p /A357

Figure 15 Variation of the stress intensity factor of the onset Mode I crack or final failure to the volume fraction.

and the final fatigue fracture depth from the specimen surfaces.

The maximum stress intensity factors of the onset of Mode I crack start and fatigue fracture toughness for SiC_p/A356 and SiC_p/A357 composites are lower than that for the SiC_w/A2024 composites. It is suggested that the effect of the whiskers on fatigue crack propagation resistance is more significant than that of SiC particles.

The ranges of stress intensity factor at fatigue threshold, ΔK_{th} , were 2.5 and 3.2 MPa m^{1/2} for SiC_w/A2124 underaged and overaged composites [9], respectively. The maximum stress intensity factor, K_{max1} at which Mode I crack starts was higher for the SiC_w/A2024 composites than the values of ΔK_{th} for the SiC_w/A2124 composites. On the other hand, the values of ΔK_{th} were about 2.9 or 4.2 MPa m^{1/2} for SiC_p/MB78 composites [10] containing fine or coarse particles, respectively. The values of K_{max1} for SiC_p/A356 or SiC_p/A357 composites were nearly equal to the ΔK_{th} value for SiC_p/MB78 composites [10] containing fine particles.

On the other hand, the fracture toughness of SiC_w/A6061 composites decreases with increasing volume fraction of SiC whiskers, while for SiC_p/MB78 [10] and SiC_p/A6061 [7] composites, the fracture toughnesses also decrease with increasing volume fraction of SiC particles. The values of K_{Ic} for

SiC_w/A2024 composites are lower than those for SiC_w/A6061 composites [7]. The minimum values of fatigue fracture toughness are about 8 MPa^{1/2} over a volume fraction of about 20% SiC whiskers or SiC particles. Those values are nearly equal to that of ceramics such as zirconia (Mg-PSZ) ($K_{IC} = 9.5 \text{ MPa m}^{1/2}$) [20]. It is considered that the fracture toughness for composites would depend on the fabrication process, matrix alloys and ageing conditions.

Although the ranges of maximum stress intensity factor from onset of Mode I cracking to final fatigue failure for these composites used in this study are very small, the values of m in the Paris equation for composites would be very large in comparison to those for unreinforced materials.

When the Mode I fatigue crack initiates, the fatigue crack would suddenly propagate to final failure. Then Mode I fatigue crack initiation is very significant for the fatigue properties of those composites. It is necessary to obtain the fatigue threshold data in order to analyse the fatigue strength of composites.

4. Conclusions

Fatigue strength was evaluated and the Mode I fatigue crack initiation and propagation mechanisms discussed for SiC_w/A2024, SiC_p/A356 and SiC_p/A357 composites.

1. The fatigue limit was clearly observed for SiC_w/A2024 composites up to about 10⁸ cycles, while for SiC_p/A356 and SiC_p/A357 composites the fatigue limit was not yet been found up to about 10⁷ cycles.

2. Fatigue strength for SiC_w/A2024 increased with increasing volume fraction of SiC whiskers compared to the matrix alloys, while for SiC_p/A357 composite the increase in fatigue strength of the matrix alloy tended to become saturated over a volume fraction of 15%. The fatigue strength of SiC_p/A356 composite tended to be a maximum at a volume fraction of 10%.

3. Stage I cracking was observed on the fatigue fracture surface of SiC_w/A2024 and SiC_p/A357 composites, while for the SiC_p/A356 composite the voids were found near the specimen surfaces, and fatigue crack would initiate from those voids. In the crack propagation region, for the SiC_w/A2024 composite, dimple patterns and striation patterns were observed, while for SiC_p/A356 and SiC_p/A357 composites near the crack origin, striation-like patterns were observed, and near the final failure, dimple patterns initiated from the silicon carbide particles.

4. A Mode I fatigue crack initiation mechanism has been proposed on the basis of the observation of fatigue fracture surfaces. For the SiC_w/A2024 composite, fatigue cracking would initiate by slip deformation, and when the crack reached the whisker-rich

zone, the fatigue crack would be arrested by the whiskers. Near the crack origin, the fatigue crack would start to form a dimple at the edge of the whiskers or intersect the whiskers. For the SiC_p/A357 composite the same mechanism was considered for the SiC_w/A2024 composite. For the SiC_p/A356 composite the fatigue crack would initiate from the voids situated beneath the specimen surfaces.

5. A fatigue crack propagation mechanism has also been proposed. When the fatigue crack reaches the whisker-rich zones the crack would be arrested by the whiskers until voids were formed at the edge of the whiskers, while for SiC particle-reinforced composites, the crack would propagate in a zig-zag fashion in order to keep away from the particles. In the case of a long crack region, the voids or subcracks would initiate around the whiskers or particles sited ahead of the main crack. The crack propagation rates would increase in comparison to the matrix alloys, due to the linkage between the main crack and the voids or subcracks situated in front of the main crack.

References

1. A. P. DIVECHA, S. G. FISHMAN and S. D. KARMARKAR, *J. Met.* **33** (1981) 12.
2. T. G. NEIH and R. F. KARLAK, *J. Mater. Sci. Lett.* **2** (1983) 119.
3. R. J. LEDERICH and S. M. L. SASTRY, *Mat. Sci. Engng* **55** (1982) 143.
4. D. F. HASSON, S. M. HOVER and C. R. CROWE, *J. Mater. Sci.* **20** (1985) 4154.
5. D. WEBSTER, *Met. Trans.* **13A** (1982) 1511.
6. D. L. McDANIELS, *ibid.* **16A** (1985) 1105.
7. S. V. NAIL, J. K. TEIN and R. C. BATES, *Int. Met. Rev.* **20** (1985) 275.
8. W. A. LOGSDON and P. K. LIAW, *Engng Fract. Mech.* **24** (1986) 737.
9. T. CHRISTMAN and S. SURESH, *Mater. Sci. Engng* **A102** (1988) 211.
10. J. K. SHANG, W. YU and R. O. RITCHIE, *ibid.* **A102** (1988) 181.
11. "Aluminium Alloys Data Sheets, A356, 1 and A357. 1" (Light Metals Information Ltd, Tokyo, 1978).
12. A. SATO and R. MEHRABIAN, *Met. Trans.* **7B** (1976) 443.
13. H. FUKUDA and TSU-WEI CHOU, *J. Mater. Sci.* **17** (1982) 1003.
14. "Metal Matrix Composites Review" (Japan New Materials Centre, Osaka 1987) p. 45.
15. T. HATTORI and S. SAKAI, MHI Report 25 (1988) 1.
16. "Fatigue Design Data for Steels and Light Metals" (Japan JSME, 1978) p. 99.
17. D. F. HASSON, C. R. CROWE, J. S. AHEARM and D. C. COOKE, *Fail. Mech. High Perform. Mater.* (1985) 231.
18. S. J. HARRIS, *Mater. Sci. Tech.* **4** (1988) 231.
19. P. J. E. FÖRSYTH, *Acta Metall.* **11** (1963) 703.
20. T. NOSE and T. FUJII, *J. Amer. Ceram. Soc.* **71** (1988) 328.

Received 24 July 1990

and accepted 6 February 1991